End-to-End Virtual MIMO Transmission in Ad Hoc Cognitive Radio Networks

I-Wei Lai, *Member, IEEE*, Chien-Lun Chen, Chia-Han Lee, *Member, IEEE*, Kwang-Cheng Chen, *Fellow, IEEE*, and Ezio Biglieri, *Life Fellow, IEEE*

***Abstract*—Ad hoc cognitive radio networks (CRNs) have the potential for meeting the challenge of increasing radio spectrum efficiency. However, traditional control of ad hoc networking demands end-to-end information channel feedback, whose feasibility is hard in ad hoc CRNs due to the opportunistic nature of spectrum access. In this paper, we propose a virtual multiple-input multiple-output (MIMO) approach to facilitate error-resilient end-to-end transmission with no need for feedback information. An erasure-channel model is used to describe the randomness of outage caused by opportunistic links. At source node, a discrete Fourier transform (DFT)-based path–time code (PTC) is used to exploit path diversity. The *a priori* erasure probability is analyzed, and a pipeline scheduling scheme with unequal waiting periods is designed to reduce such probability. At destination node, knowledge of the *a priori* erasure probability is exploited to overcome the decoding challenge raised by the presence of random erasures. A joint sphere decoder (JSD) with a minimum mean-squared error sorted QR decomposition (MMSE-SQRD) effectively implements maximum *a posteriori* (MAP) probability decoding. This decoder simultaneously performs erasure identification and data decoding. Numerical results show that the proposed virtual MIMO framework can pave the way to efficient and reliable end-to-end transmission in ad hoc CRNs.**

***Index Terms*—Multiple-input multiple-output (MIMO), virtual MIMO, cognitive radio network (CRN), ad hoc networks, erasure channel, path–time code (PTC), sphere decoder (SD), QR decomposition (QRD).**

I. Introduction

COGNITIVE radio (CR) has been widely regarded as a key technology to enhance the spectrum utilization in wireless communications [1]–[5]. While a primary user has exclusive privilege to access its licensed channels, a CR is capable of dynamically adapting its parameters to make best use of the available spectrum without interfering with the primary users. Formed by primary users and CRs, ad hoc cognitive radio networks (CRNs) aim at improving the end-to-end communication performance without centralized control.

Although spectrum efficiency is greatly enhanced by employing CR, the node-to-node CR links are opportunistic and thus random due to the following reasons: First, to avoid interfering with primary users or other CRs, a relay node must buffer the CR packet and sense the availability of the link to its next node before forwarding. The transmission delay is prolonged when the spectrum is heavily used so that available links are scarce. The CR packets experiencing a long transmission delay beyond the time-to-live threshold are discarded before arriving at the destination node [6]. Second, practically vulnerable spectrum sensing results in severe interference or collisions when a node forwards CR packets to a link occupied by other CRs or the primary users.

Many routing algorithms have been proposed [7]–[10] which aimed at precise control of ad hoc CRNs. For example, joint design of routing, spectrum sensing, scheduling, and resource allocation is considered [7], [8] to optimize the end-to-end performance of CRs. Other than the complexity of such joint design, these routing algorithms of ad hoc CRNs usually demand end-to-end information. However, since the opportunistic links in ad hoc CRNs are random, unreliable and therefore likely unidirectional [6], [11], end-to-end information exchange, which assumes a control channel and a feedback link, requires tremendous control overhead. This control overhead makes the algorithms not scalable to a large ad hoc CRN [12]. On the other hand, by utilizing only the local information [13]–[15], routing can be established in a *statistical* manner, implying that the presences of random availability of the links are allowed. To combat this intrinsic randomness, the error-resilient end-to-end transmission should be developed [12], [16].

In this paper, we propose to design the error-resilient end-to-end transmission not requiring any feedback information. To retain such error control resilience over ad hoc CRNs, multi-path end-to-end transmission should be established [17]–[19]. In particular, by encoding packets along both path and time coordinates [20], the end-to-end transmission of ad hoc CRNs is formulated as a new type of *virtual multiple-input multiple-output (MIMO)* technology. Conventional virtual MIMO technology has multiple cooperating source nodes communicating

Manuscript received March 22, 2013; revised July 31, 2013; accepted September 14, 2013. The associate editor coordinating the review of this paper and approving it for publication was W. Zhang.

I-W. Lai and C.-H. Lee are with the Research Center for Information Technology Innovation, Academia Sinica, Taipei, Taiwan (e-mail: {iweilai, chiahan}@citi.sinica.edu.tw).

C.-L. Chen is with the Ming Hsieh Department of Electrical Engineering, University of Southern California (USC), Los Angeles, California, USA (e-mail: chienlun.chen@gmail.com).

K.-C. Chen is with the Graduate Institute of Communication Engineering, National Taiwan University, Taipei, Taiwan (e-mail: chenkc@cc.ee.ntu.edu.tw).

E. Biglieri is with the Universitat Pompeu Fabra, Barcelona, Spain, and King Saud University, Riyadh, KSA (e-mail: e.biglieri@ieee.org).

The work of Ezio Biglieri was supported by Project TEC2012-34642 and by the Distinguished Scientist Fellowship Program at King Saud University. Chia-Han Lee and Kwang-Cheng Chen were supported by the National Science Council, National Taiwan University, and INTEL Corp. under the contract NSC 101-2219-E-002-023, NSC 102-2221-E-002-016-MY2, and 102R3401-2.

Digital Object Identifier 10.1109/TWC.2013.112513.130519

with multiple destination nodes [21], [22]. In our framework, multiple nodes are used to form multiple relay paths between a source/destination node pair. The relay paths aggregate to form a new "channel" at the *network* level (more specifically, at *session* level since we can imagine an end-to-end session on top of the end-to-end multipath transmission). Based on this formulation, new encoding/decoding schemes at the network layer, enabling error-resilient end-to-end transmission in ad hoc CRNs, can be developed by exploiting what has been done in physical-layer MIMO research. This way, the end-to-end virtual MIMO transmission only requires local sensing, and thus eliminates the need of end-to-end feedback and control. Note that although the distributed space–time code [23]–[26] or distributed spatial multiplexing [27] also applies the physical-layer MIMO techniques to the network layer, the randomness in ad hoc CRNs makes our scheme of designing encoding/decoding on the network layer fundamentally much more challenging.

Compared with physical-layer MIMO systems [28], the major design challenge of end-to-end virtual MIMO transmission in ad hoc CRNs lies in the random outage of transmissions due the packet expiration, severe interference, and deep fading. The erasure MIMO channel is adopted to model transmission outages. This model involves an erasure matrix whose entries are independent Bernoulli random variables [29]. Notice that erasures resulting from a single source may be correlated, which makes statistical modeling of erasures coming from multiple sources a potentially very complicated task. To overcome this difficulty, we assume independent erasures, which should prove to be a reasonable approximation. Then, a path–time code (PTC) [20] is designed to encode the packets along path and time coordinates. Discrete Fourier transform (DFT) is the tool used in path–time coding to combat time-varying erasures. Specifically, the DFT matrix reflects the frequency behavior of the fading gains of relay paths. When a fading gain in a time slot happens to be nonzero, its frequency components are nonzero as well, and hence packets transmitted on these frequencies are less likely to be erased, thus increasing the transmission diversity.

To allow the CR to have more chances to sense/access the opportunistic links, a coded packet is immediately transmitted before its previous coded packet arrives at the destination node, similar to the pipeline architecture in hardware implementation. This pipeline scheduling scheme effectively lowers the erasure probability. However, in this situation, a CR can transmit multiple coded packets simultaneously through a relay path, thus resulting in the queueing of these coded packets. The resulting queueing can be modeled using series queues [30], which complicates the analysis of erasure probability compared to the traditional scenario. Note that the knowledge of the value of this *a priori* erasure probability not only is crucial for performance evaluation, but can also be utilized to enhance end-to-end performance. For example, while conventionally waiting periods of coded packets are assumed to be equal, the destination node can utilize the analytical *a priori* erasure probability to optimize the waiting periods.

After receiving the coded packets, the destination node encounters the main end-to-end transmission challenge in the ad hoc CRN, i.e., the presence of random erasures. We advocate the use of a joint sphere decoding (JSD) algorithm with the maximum *a posteriori* (MAP) probability criterion to jointly identify the presence of erasures and decode the data. In particular, JSD exploits the knowledge of the *a priori* erasure probability to perform the optimal joint detection. Owing to erasures, ill-conditioned channel matrices, which cause an increase of the decoding complexity, occur more frequently than in physical-layer MIMO systems. For complexity reduction, a minimum mean-squared error sorted QR decomposition (MMSE-SQRD) is used to regularize the channel matrix. In combination with MMSE-SQRD, JSD achieves reliable end-to-end transmission with viable decoding complexity.

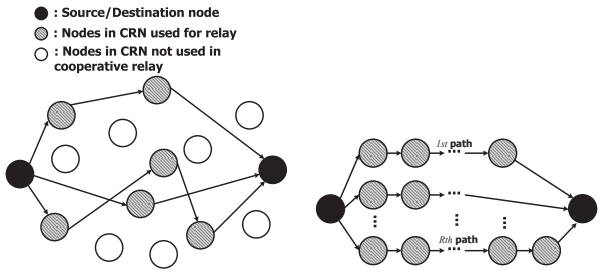

(a) Example topology of a multihop ad hoc CRN. (b) Equivalent directed graph model.

Fig. 1. Example topology of end-to-end transmission in an ad hoc multihop CRN.

In short, the contributions of this paper are listed as follows:

- Formulation of a novel virtual MIMO technology "over" ad hoc CRNs which provides error-resilient end-to-end transmission without requiring feedback and end-to-end information.
- PTC based on DFT that encodes the packet to exploit path diversity for the end-to-end transmission.
- A pipeline scheduling scheme with unequal waiting periods that lowers the erasure probability in the end-to-end transmission, which is verified by comprehensive analysis.
- Combination of JSD and MMSE-SQRD to jointly identify the presence of erasures and decode the data packet to achieve a satisfactory and robust end-to-end error rate performance (this differs from traditional error correction at physical layer).

The paper is organized as follows: Section II describes the virtual-MIMO system and the erasure-channel model. Section III focuses on PTC. Section IV introduces the pipeline scheduling scheme and the analysis of erasure probability. Section V elaborates on JSD and MMSE-SQRD. Section VI provides numerical results to validate the analysis and to demonstrate the performance of the proposed virtual MIMO techniques. Finally, conclusions are drawn in Section VII.

II. Virtual MIMO Formulation

Let us call *link* the connection between two nodes, and *path* the connection route between source and destination nodes, i.e., the end-to-end connection. This multihop networking can be viewed as R link-disjoint paths [16], [31], which respectively comprise $N_r - 1$ cognitive radio relay

nodes, $r \in \{1, \ldots, R\}$, have been established by using any of the routing algorithms from [17]–[19]. Fig. 1(a) illustrates an example of the network topology of the constructed multipath routes, and Fig. 1(b) depicts its equivalent directed-graph model. The cognitive relays over different links on different paths can transmit simultaneously since the availability of any two links in two different paths is independent, due to the link-disjoint condition. After establishing the multiple relay paths, the source node encodes the data along both time and path coordinates. The coded packets are then transmitted to different relay paths by applying multiplexing techniques or the two-step protocol [25]. The coded packet in each relay path is then amplified and forwarded toward the destination node. The scheduling is performed in a distributed manner: The relay node amplifies and forwards the received coded packets toward the destination node, given that the life time of the coded packet does not expire; the expired coded packet is discarded, which causes an *erasure*. An erasure also happens when the coded packets experience deep fading or severe interference from primary users/other CRs due to imperfect spectrum sensing or simultaneous transmissions of multiple CRs. By collecting the PTC-coded packets, the destination node identifies the presence of erasures and decodes the data.

Now let us define the *waiting period* as the period during which the destination node is assumed to receive the associated coded packet. With a longer waiting period, a relay node is allowed to make more attempts to sense and access the opportunistic links. If all the links can be sequentially accessed within the waiting periods, the coded packet can reach the destination; otherwise, it is discarded and an erasure occurs. Define B as the length of a PTC code word, i.e., the number of coded packets used to transmit a data packet. An *erasure matrix* $\mathbf{V} \in \{0,1\}^{B\times R}$ is defined to describe the positions and the number of erasures: specifically, its (b,r)th entry $v_{b,r}$ is a Bernoulli random variable [29] taking value 0 when an erasure occurs at the rth path and the bth time instant.

For the end-to-end coded CRN transmission using the PTC, we focus on unit-rate PTCs, so that the transmission rate is not reduced. Defining χ as the constellation set, the source node encodes a data packet $\mathbf{x} \in \chi^B$ by a coding matrix $\tilde{\mathbf{C}}_b \in \mathbb{C}^{R\times B}$ and transmits the resulting coded packet at time instant b. Define $\mathbf{v}_b = [v_{b,1}, \ldots, v_{b,R}]$, $\mathbf{g}_b = [g_{b,1}, \ldots, g_{b,R}] \in \mathbb{C}^R$ as the path fading gain vector at time instant b, and their Schur product $\mathbf{g}_b \circ \mathbf{v}_b = [g_{b,1}v_{b,1}, \ldots, g_{b,R}v_{b,R}]$. With these definitions, the received coded packet at the destination node has the form

$$y_b = (\mathbf{g}_b \circ \mathbf{v}_b)^\top \tilde{\mathbf{C}}_b \mathbf{x} + \sum_{r=1}^{R} \tilde{n}_{b,r} = (\mathbf{g}_b \circ \mathbf{v}_b)^\top \tilde{\mathbf{C}}_b \mathbf{x} + n_b, \quad (1)$$

where $(\cdot)^\top$ denotes transposition, $\tilde{n}_{b,r}$ is the noise aggregated from all links in the rth path, and $n_b = \sum_{r=1}^{R} \tilde{n}_{b,r}$. Due to relay link gains, the noise variance of the additive white Gaussian noise (AWGN) $\tilde{n}_{b,r}$ is different for every r and b [25]. Therefore, n_b is also AWGN with time-varying noise power spectral density $N_{0,b}$. We assume that $g_{b,r}$ is known at the destination node, but neither the source nor destination node has information of $v_{b,r}$. The destination node is responsible for identifying the presence of erasures, in additional to decoding data packet.

The received coded packet from $b = 1$ to $b = B$ can be represented as

$$\mathbf{y} = \underbrace{\begin{bmatrix} (\mathbf{g}_1 \circ \mathbf{v}_1)^\top & \ldots & \mathbf{0}^T \\ \vdots & \ddots & \vdots \\ \mathbf{0}^T & \ldots & (\mathbf{g}_B \circ \mathbf{v}_B)^\top \end{bmatrix} \begin{bmatrix} \tilde{\mathbf{C}}_1 \\ \vdots \\ \tilde{\mathbf{C}}_B \end{bmatrix}}_{\mathbf{C}} \mathbf{x} + \underbrace{\begin{bmatrix} n_1 \\ \vdots \\ n_B \end{bmatrix}}_{\mathbf{n}}$$

$$= \underbrace{\begin{bmatrix} (\mathbf{g}_1 \circ \mathbf{v}_1)^\top \tilde{\mathbf{C}}_1 \\ \vdots \\ (\mathbf{g}_B \circ \mathbf{v}_B)^\top \tilde{\mathbf{C}}_B \end{bmatrix}}_{\mathbf{H}_{\text{eq}}(\mathbf{V},\mathbf{C})} \mathbf{x} + \mathbf{n} = \mathbf{H}_{\text{eq}}(\mathbf{V}, \mathbf{C})\mathbf{x} + \mathbf{n}, \quad (2)$$

where $\mathbf{C} = [\tilde{\mathbf{C}}_1^\top \ \ldots \ \tilde{\mathbf{C}}_B^\top]^\top \in \mathbb{C}^{RB\times B}$ represents the cascaded $\tilde{\mathbf{C}}_b$. With the formulation in (2), the end-to-end coded ad hoc CRN system is described by the same equation as a symmetric spatial multiplexing MIMO system, characterized by the equivalent channel matrix $\mathbf{H}_{\text{eq}}(\mathbf{V}, \mathbf{C}) \in \mathbb{C}^{B\times B}$. This matrix incorporates RB Bernoulli random variables modeling the erasures, and, as the channel matrix of a MIMO system, can be modified by a suitable choice of the coding scheme [32, p. 350 ff.]. In conclusion, (2) can be interpreted as describing a virtual MIMO system where multiple nodes are coordinated to form multiple relay paths between a source/destination node pair. The source node encodes the data packet along time and path coordinates, thus shaping $\mathbf{H}_{\text{eq}}(\mathbf{V}, \mathbf{C})$. The destination node has to decode the B constellation points in $\mathbf{x}$, given that the received coded packets are impaired by the erasures modeled by the RB Bernoulli random variables contained in $\mathbf{V}$.

III. Path–Time Code

PTCs aim at exploiting path and time diversity to improve the transmission reliability [20], just as space–time codes function in the physical layer. However, due to the presence of erasures caused by the opportunistic links, the design of PTCs is more challenging, especially when time-varying erasures need to be accounted for.

A. Permutation and Orthonormal Matrices for PTCs

We first investigate PTCs to be used on a channel where erasures remain constant during B time slots, i.e., for the whole duration of a PTC code word [20]. For uncoded transmission, every erasure nulls a column of $\mathbf{H}_{\text{eq}}(\mathbf{V}, \mathbf{C})$, and thus an element of $\mathbf{x}$ is lost. To mitigate this, coding matrices are introduced to make the entries in $\mathbf{v}_b$ uniformly distributed across the columns of $\mathbf{H}_{\text{eq}}(\mathbf{V}, \mathbf{C})$. Specifically, if $R = B$, the identity matrix is used as $\tilde{\mathbf{C}}_1$. For $b \geq 2$, the coding matrix $\tilde{\mathbf{C}}_b$ is generated by circularly shifting the row vectors of $\tilde{\mathbf{C}}_{b-1}$ up (or down). A set of coding matrices is therefore constructed in the form of permutation matrices, which effectively lowers the error floor [20].

According to the design criterion advocated in [33], the path diversity is bounded by the minimum distance between any pairs of coded packets $\mathbf{C}\hat{\mathbf{x}}$ and $\mathbf{C}\check{\mathbf{x}}$, where $\hat{\mathbf{x}}$ and $\check{\mathbf{x}}$ are two arbitrary data packets. This implies that, even if null columns are avoided, the null entries in $\mathbf{H}_{\text{eq}}(\mathbf{V}, \mathbf{C})$ still impair the performance. Based on this observation, we propose the use

of orthonormal matrices to increase the path diversity. For simplicity's sake, considering a CRN with $R = B = 4$, the first coding matrix is the orthonormal matrix

$$\tilde{\mathbf{C}}_1 = \frac{1}{2}\begin{bmatrix} 1 & 1 & 1 & 1 \\ -1 & 1 & -1 & 1 \\ -1 & 1 & 1 & -1 \\ -1 & -1 & 1 & 1 \end{bmatrix}. \tag{3}$$

The remaining code matrices are generated in the same way as with permutation coding. As shown in [20], PTCs with orthonormal matrices outperform those with permutation matrices by several dB of signal-to-noise ratio (SNR).

Now, in a fast-erasure channel, where $v_{b,r}$ takes independent values at different time instants b, the performance of both families of PTCs is deteriorated. Consider for example the case with $R = B = 2$ and orthonormal PTC. If $v_{1,1}$ and $v_{2,2}$ are null, $\mathbf{H}_{\text{eq}}(\mathbf{V}, \mathbf{C})$ becomes a rank deficient matrix. For example,

$$\mathbf{H}_{\text{eq}}\left(\begin{bmatrix} 0 & 1 \\ 1 & 0 \end{bmatrix}, \frac{1}{\sqrt{2}} \begin{bmatrix} 1 & 1 \\ 1 & -1 \\ 1 & -1 \\ 1 & 1 \end{bmatrix} \right) = \frac{1}{\sqrt{2}} \begin{bmatrix} g_{1,2} & -g_{1,2} \\ g_{2,1} & -g_{2,1} \end{bmatrix}. \tag{4}$$

Therefore, new criteria for designing PTCs must be found in the following subsection when dealing with a fast-erasure channel.

B. DFT-Based PTC

A drawback of orthonormal PTCs lies in the fact that different $\tilde{\mathbf{C}}_i$ are formed from the same group of row vectors. As the example shown in (4), the nonzero $v_{1,2}$ and $v_{2,1}$ retain the identical second and third row vectors of $\mathbf{C}$, making $\mathbf{H}_{\text{eq}}(\mathbf{V}, \mathbf{C})$ rank deficient. Thus, the DFT-based PTC which comprises distinct row vectors is proposed to resolve this. The DFT-based PTC is generated by applying code matrices with the (k, b)th entry, $C_{k,b}$, being

$$C_{k,b} = \frac{1}{\sqrt{R}} e^{\frac{-j2\pi kb}{RB}}, \qquad k = 1, \ldots, RB, \qquad b = 1, \ldots, B, \tag{5}$$

where the normalization factor $\sqrt{R}$ accounts for the fact that the packet is transmitted through R opportunistic paths. As the DFT transforms a function of time into the frequency spectrum of this function, the DFT-based PTC can be interpreted in a similar way as the following. From (2), we have the time-domain channel impulse response at the bth time instant

$$[\underbrace{\mathbf{0}^\top \ldots \mathbf{0}^\top}_{b-1} (\mathbf{g}_b \circ \mathbf{v}_b)^\top \underbrace{\mathbf{0}^\top \ldots \mathbf{0}^\top}_{B-b}]. \tag{6}$$

After processing by the DFT-based PTC, the bth row vector of $\mathbf{H}_{\text{eq}}(\mathbf{V}, \mathbf{C})$ indicates the channel frequency response of (6). As long as $\mathbf{v}_b \neq \mathbf{0}$, all the entries of the bth row vector of $\mathbf{H}_{\text{eq}}(\mathbf{V}, \mathbf{C})$ are nonzero. In this case, $\mathbf{x}$ are received unerased at time b, which results in increased diversity.

The use of DFT matrices as code matrices has several upsides, viz.,

- Since all the entries in $\mathbf{C}$ are nonzero, every x_b is dispersed to all paths at all B time instants. Given two data packets that differ in a certain entry x_b, the Hamming distance of the associated PTC coded packets is maximized to RB.
- Distinct row vectors avoid the rank-deficiency problem in (4).
- They allow implementation by fast Fourier transform (FFT) architectures, such as those widely used in orthogonal frequency-division multiplexing (OFDM) systems.

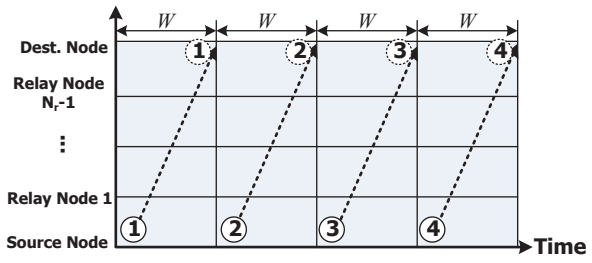

(a) Conventional scheduling scheme; W is the waiting period.

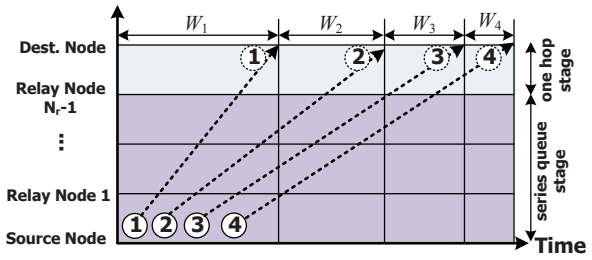

(b) Pipeline scheduling scheme with unequal waiting periods; W_b indicates the waiting period of the bth code packet.

Fig. 2. Timing diagrams of conventional scheduling and pipeline scheduling with unequal waiting periods.

IV. SCHEDULING

In a conventional ad hoc CRN, when, due to an occupied link, a coded packet experiences an end-to-end delay longer than the waiting period, this coded packet is discarded. In this section we introduce a novel scheduling scheme that allows coded packet to tolerate end-to-end delay longer than the waiting period. A systematic analysis of erasure probability is also provided. Note that since the scheduling addressed in this section only reduces the probability of packet expiration, erasures caused by deep fading or strong interference are ignored in the analysis. For notational brevity, in this section we omit the subscript r which indexes the path.

A. Conventional Scheduling Scheme

Assume a transmission latency relatively small compared with the delay caused by the unavailability of occupied links.

Given perfect timing information at all nodes[1], each transmission is nonoverlapped as illustrated in Fig. 2(a). We define the sensing interval as the period during which a relay node can sense the link availability once. The normalized waiting period W (normalized with respect to the sensing interval) indicates the overall number of sensing that the nodes are allowed to perform for the N opportunistic links. Since nodes have perfect timing information, the distributed scheduling is straightforward: each node simply performs sensing at the beginning of every sensing interval. Once the end-to-end delay exceeds the waiting period, the coded packet is discarded. Sequential sensing of the N opportunistic links can be modeled as a Bernoulli trial, characterized by the geometrically distributed random, variable $G(\delta)$, where δ is the probability of a link occupied by primary users or other CRs. Since the end-to-end delay is the summation of N geometric random variables, it follows a negative binomial distribution $\mathrm{NB}(N,\delta)$ with probability mass function (PMF)

$$P_{\mathrm{NB}}(x;N,\delta)=\left(\begin{array}{c}x+N-1\\N-1\end{array}\right)(1-\delta)^N\delta^x. \tag{7}$$

When the end-to-end delay τ is shorter than the waiting period W, we have path availability (i.e., $v_b=1$) with probability given by [16]

$$P(v_b=1)=P(\tau\le W)=\sum_{\tau=N}^{W}P_{\mathrm{NB}}(\tau-N;N,\delta). \tag{8}$$

As illustrated in Fig. 2(a), a drawback of the conventional scheduling scheme lies in the fact that only one of the opportunistic links of a relay path is utilized, while there may be multiple links concurrently available. This sensing strategy does not fully exploit the opportunistic transmission concept since most of the relay nodes are idle.

B. Pipeline Scheduling Scheme with Unequal Waiting Periods

To improve the utilization of the opportunistic links, we propose a *pipeline scheduling* scheme which transmits one coded packet immediately after another at every sensing interval as depicted in Fig. 2(b). Using pipeline scheduling, the erasure probability decreases, as CRs can simultaneously sense/access multiple opportunistic links in one path.

Although pipeline scheduling is simple and effective, we hasten to point out that it introduces two extra delays, which degrade its potentially superior performance. First, as multiple coded packets are now simultaneously transported in the relay path, congestions and queueing occur. Second, coded packet should arrive at their specific waiting periods since the destination node identifies the received coded packet by its arrival time, as depicted in Fig. 2(b). Therefore, early-arrival coded packet is proposed to be buffered in the last node closest to destination in each path, even when an opportunistic link to the destination node is available.

Given these two delays, an end-to-end transmission using pipeline scheduling can be treated as two stages, viz.,

Series-Queue Stage [30] [2]: $N-1$ opportunistic links, where congestions among coded packets may occur.

One-Hop Stage: The single opportunistic link connected to the destination node.

As shown in Fig. 2(b), the pipeline scheduling scheme effectively prolongs the permissible end-to-end delay of all coded packets after the first one. The first several coded packets have a higher erasure probability than the others, and dominate the scheme performance. This unbalance of erasure probabilities can be mitigated by increasing the waiting periods of the first coded packets. We call this scheme *pipeline scheduling with unequal waiting periods*. To elaborate on this scheme, in the sequel the erasure probability will be analyzed, and the distribution of the waiting periods optimized. As we shall see, the connected decoding algorithm requires knowledge of the *a priori* erasure probability to perform MAP decoding.

C. Analysis of Erasure Probability

Define k_b as the number of links that the bth coded packet encounters which are unavailable due to congestions among coded packets. We analyze the erasure events in three steps. First, the erasure probability conditioned on k_b is derived. Next, we derive the PMF of k_b from a toy example with $N=2$, i.e., one link in the series-queue stage. Finally, the general case $N>2$ is discussed. For simplicity and clarity's sake, in this subsection we restrict ourselves to a treatment of equal waiting periods only. The case of the unequal waiting periods can be easily handled by generalizing the derivation in this subsection.

1) Derivation of $P(v_b \mid k_b)$: As shown in Fig. 2(b), the transmission of the first coded packet using pipeline scheduling occurs just as in a conventional scheme, since the maximum end-to-end delay equals the waiting period, and $k_b=0$. Therefore, $P(v_1=1)$ is the same as in (8):

$$P(v_1=1)=P(\tau\le W)=\sum_{\tau=N}^{W}P_{\mathrm{NB}}(\tau-N;N,\delta). \tag{9}$$

For $b\ge 2$, we have $k_b\ge 0$, since the bth coded packet might arrive at a link where the $(b-1)$th coded packet is still queued. The probability of path availability has the form

$$P(v_b=1)=\sum_{k_b=0}^{(b-1)(W-1)}P(v_b=1\mid k_b)P(k_b), \tag{10}$$

where $P(k_b)$ denotes the PMF of k_b. The maximum value of k_b is $(b-1)(W-1)$, which is taken when the previous $(b-1)$th coded packet has left the path at the $(b-1)W$th sensing interval, and the current bth coded packet is transmitted at the $(b-1)$th sensing interval, as illustrated in Fig. 2(b).

To compute $P(v_b=1|k_b)$, we take the product of the probabilities that the bth coded packet passes the series-queue

[1]We assume all nodes perform synchronization once before the end-to-end transmission, in order to have the timing information, i.e., the sensing and waiting periods. However, the actual operation of this proposed virtual MIMO technology does not really assume the need of synchronization due to its sequential (event-driven) operation. Synchronization among nodes may significantly simplify analysis of sensing and performance. Please note that the work in [34] suggests that asynchronous operation does not necessarily imply performance loss, at the price of extra implementation design.

[2]In the *series queue* [30] coded packet sequentially passes through several CR relay nodes, with a delay distribution $G(\cdot)$.

stage and the one-hop stage. Specifically, define the delay in the one-hop stage as $\tau_2 \in \{1, \ldots, W\}$ ($\tau_2 \leq W$ because a coded packet is allowed to be transmitted through the link connected to the destination node only within its waiting period) and the delay in the series-queue stage as $\tau_1 \in \{N-1, \ldots, b(W-1) - \tau_2 - k_b\}$. Then, $P(v_b = 1 \mid k_b)$ is given by

$$P(v_b = 1|k_b) = \sum_{\tau_2=1}^{W} \sum_{\tau_1=N-1}^{b(W-1)-\tau_2-k_b} P(v_b = 1|k_b, \tau_1, \tau_2) = \sum_{\tau_2=1}^{W} \sum_{\tau_1=N-1}^{b(W-1)-\tau_2-k_b} P_{\text{NB}}(\tau_1 - N - 1; N-1, \delta) P_{\text{NB}}(\tau_2 - 1; 1, \delta), \quad (11)$$

where $P_{\text{NB}}(\tau_1 - N - 1; N-1, \delta)$ and $P_{\text{NB}}(\tau_2 - 1; 1, \delta)$ denote the probability of passing the series-queue stage and the one-hop stage, respectively. After inserting (11) into (10), the probability that a coded packet can get through all the links within the waiting periods can be computed as long as $P(k_b)$ is available.

2) Derivation of $P(k_b)$ with $N = 2$: Define $\tilde{k}_b$ as the number of links that the bth coded packet encounters and that are unavailable because of the activity of primary users or other CRs. The PMF of $\tilde{k}_b$ is described by the negative binomial distribution

$$P(\tilde{k}_b) = \begin{cases} P_{\text{NB}}(\tilde{k}_b; 1, \delta), & \text{otherwise,} \\ \sum_{i=(b-1)(W-1)}^{\infty} P_{\text{NB}}(i; 1, \delta), & \text{if } \tilde{k}_b = (b-1)(W-1), \end{cases} \quad (12)$$

where $P(\tilde{k}_b = (b-1)(W-1))$ cumulates the tail of the negative binomial PMF since the maximum values of $\tilde{k}_b$ and k_b are identical.

For $N = 2$, only one opportunistic link exists in the series-queue stage. Once this link is unavailable for any reason, congestion occurs, and the resulting delay propagates to the following coded packets. Thus, k_b can be computed by cumulating $\tilde{k}_b$:

$$k_b = \sum_{i=1}^{b-1} \tilde{k}_i \quad (13)$$

which allows the recursive representation

$$k_b = k_{b-1} + \Delta k_{b-1}, \quad (14)$$

where $\Delta k_{b-1} \triangleq \tilde{k}_{b-1}$ when $N = 2$.

Since $k_1 = 0$, we have $P(k_2) = P(\tilde{k}_1)$ as shown in (12). For $b \geq 2$, $P(k_b)$ can be computed from the convolution of $P(k_{b-1})$ and $P(\Delta k_{b-1})$ due to (14):

$$P(k_b) = \begin{cases} \sum_{j=0}^{(b-1)(W-1)} P(\Delta k_{b-1} = j) P(k_{b-1} = k_b - j), & \text{otherwise,} \\ \sum_{i=(b-1)(W-1)}^{\infty} \sum_{j=0}^{(b-1)(W-1)} P(\Delta k_{b-1} = j) P(k_{b-1} = i - j), & \text{if } k_b = (b-1)(W-1). \end{cases} \quad (15)$$

TABLE I
EXAMPLE OF THE PMF DERIVATION OF k_1; $W_b = 4$ FOR ALL SENSING RESULTS AND $N = 3$.

Sensing results ($\mathbf{u}_1$)	$P(\mathbf{u}_1)$	$\tilde{k}_1$	Δk_1	$P(\Delta k_1 \mid \mathbf{u}_1)$
111X	$(1-\delta)^3$	0	0	1
110X	$(1-\delta)^2\delta$	0	0	1
101X	$(1-\delta)^2\delta$	1	0, 1	δ, $(1-\delta)$
100X	$(1-\delta)\delta^2$	2	0, 1, 2	δ^2, $(1-\delta)\delta$, $(1-\delta)$
011X	$(1-\delta)^2\delta$	1	1	1
010X	$(1-\delta)\delta^2$	2	1, 2	δ, $(1-\delta)$
001X	$(1-\delta)\delta^2$	2	2	1
000X	δ^3	3	3	1

3) Derivation of $P(k_b)$ with $N > 2$: In the general case $N > 2$, coded packets may be queued on different links in the series-queue stage. Even when the $(b-1)$th coded packet encounters an occupied link by the activities of other CRs or the primary users, i.e., $\tilde{k}_{b-1} > 0$, we still have $k_b = 0$ given that the upcoming bth coded packet is also queued on another link, implying that $\Delta k_b \leq \tilde{k}_b$. In this case, Δk_b critically depends on the sensing results of successive coded packets, and a case-by-case computation of Δk_b is necessary. We propose a systematic approach to this calculation, as illustrated by the simple example of Table I, which refers to the case $b = 1$, $W = 4$, $N = 3$, that is, two links in the series-queue stage.

Define the four-bit vector $\mathbf{u}_1$ describing the sensing results of the first coded packet. Each bit takes value '1' if the coded packet accesses an opportunistic link, and value '0' if the link is occupied by the primary users or other CRs. The value of the last-position bit is 'don't care (X)' since the coded packet will leave, or will be discarded from, the relay path when the end-to-end delay equals or exceeds W. The PMF of $\mathbf{u}_1$ is obtained by counting the number of '1's and '0's in $\mathbf{u}_1$ and using the results as exponents of $(1-\delta)$ and δ, respectively:

$$P(\mathbf{u}_1) = (1-\delta)^{\|\mathbf{u}_1\|_0} \delta^{(W-1-\|\mathbf{u}_1\|_0)}, \quad (16)$$

where $\|\cdot\|_0$ denotes the l^0-norm (or Hamming weight) of a vector which represents the number of its nonzero entries.

Since now the series-queue stage contains two links, $\tilde{k}_1$ is computed by counting the number of '0's before the second '1'. The results are listed in the third column in Table I. The fourth column lists Δk_1, which is obtained as follows: For the first two rows, $\Delta k_1 = 0$ since the first coded packet has passed the links without any queueing. For the third row, the first coded packet immediately passes the first link, but is queued on the second link for one sensing interval. If the second coded packet also immediately passes the first link, we have $\Delta k_1 = 1$; otherwise, we have $\Delta k_1 = 0$ as the second coded packet is queued on the first link. The associated conditional PMFs are $P(\Delta k_1 = 1 \mid \mathbf{u}_1 = 101\text{X}) = 1 - \delta$ and $P(\Delta k_1 = 0 \mid \mathbf{u}_1 = 101\text{X}) = \delta$. Likewise, for the fourth row, $\Delta k_1 = 0, 1$, or 2 with probability δ^2, $(1-\delta)\delta$, and $(1-\delta)$, depending on the sensing results of the second coded packet. The values of Δk_1 in the remaining rows can be illustrated in a similar way. The associated conditional PMF $P(\Delta k_1 \mid \mathbf{u}_1)$ is shown in the last column of Table I.

By using this systematic approach to obtain $P(\mathbf{u}_1)$

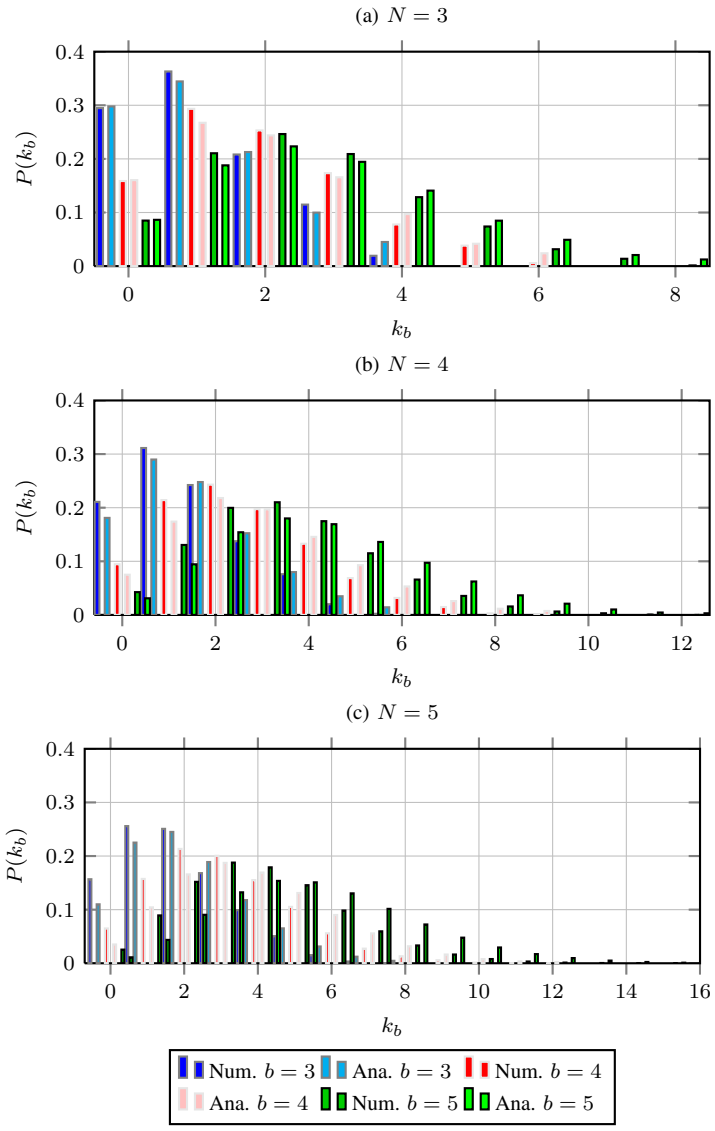

Fig. 3. Validation of the approximate PMF of k_b. The parameters used are $\delta = 0.3$ and equal waiting period $W = N$ for each subfigure.

and $P(\Delta k_1 \mid \mathbf{u}_1)$, the PMF $P(\Delta k_1)$ can be computed as

$$P(\Delta k_1) = \sum_{\mathbf{u}_1} P(\Delta k_1 \mid \mathbf{u}_1) P(\mathbf{u}_1). \tag{17}$$

Then, we have $P(k_2) = P(k_1 + \Delta k_1) = P(\Delta k_1)$. For $b \geq 2$, the method illustrated in Table I yields an approximation of Δk_b, because the sensing result $\mathbf{u}_b$ makes the assumption $k_b = 0$, which only holds true for $b = 1$.

Fig. 3 illustrates the accuracy of this approximation by comparing the analytical $P(k_b)$ with its numerical results under the condition of various b, N, and $\delta = 0.3$, assuming that the CRN doubles the current spectral efficiency [35]. The normalized waiting period W is set to be identical to the number of opportunistic links N, which is the minimum requirement for the first coded packet to pass the N-link path. As can be seen, our approximation yields a result close to exact in most configurations with $N = 3$ and 4. The accuracy decreases as b and N increase, e.g., the situation where the fifth coded packet of a long PTC code word is transported in a long relay path comprising five opportunistic links. By using the approximate $P(k_b)$, (10), and (11), the *a priori* erasure probability is able to be accurately estimated.

V. MAP Decoding

At destination node, the operation of the virtual MIMO decoder is much more complicated than at physical layer. Specifically, a straightforward decoder implementation would need $2^{RB} - 1$ sets of physical-layer MIMO decoders, because the possible realizations of the random-erasure matrix $\mathbf{V}$ are in number of $2^{RB} - 1$ (the '-1' accounts for the exclusion of $\mathbf{V} = \mathbf{0}$). A new decoding algorithm is consequently called for.

A. MAP Joint Detection

We assume that the elements $\mathbf{x}$ of a coded packet are randomly selected from χ with the same probability $P(\mathbf{x}) = |\chi|^{-B}$, where $|\chi|$ is the cardinality of χ. However, as discussed in Section IV, $\mathbf{V}$ is not uniformly distributed. Thus, it is appropriate to choose a decoding algorithm based on the MAP criterion, viz.,

$$\begin{aligned}(\hat{\mathbf{x}}, \hat{\mathbf{V}}) &= \underset{\mathbf{x}\in\chi^B, \mathbf{V}\in\{0,1\}^{RB}}{\arg\max} P(\mathbf{x}, \mathbf{V} \mid \mathbf{y}) \\ &= \underset{\mathbf{x}\in\chi^B, \mathbf{V}\in\{0,1\}^{RB}}{\arg\max} P(\mathbf{y} \mid \mathbf{x}, \mathbf{V}) P(\mathbf{x}) P(\mathbf{V}). \end{aligned} \tag{18}$$

Since n_b is AWGN with the noise power spectral density $N_{0,b}$, we obtain

$$P(\mathbf{y} \mid \mathbf{x}, \mathbf{V}) = \frac{1}{\pi^B \prod_{b=1}^{B} N_{0,b}} e^{\|\mathrm{diag}(\boldsymbol{\rho})\mathbf{y} - \mathrm{diag}(\boldsymbol{\rho})\mathbf{H}_{\mathrm{eq}}(\mathbf{V},\mathbf{C})\mathbf{x}\|^2}, \tag{19}$$

where $\mathrm{diag}(\boldsymbol{\rho})$ indicates a diagonal matrix with diagonal terms $\boldsymbol{\rho} = [1/\sqrt{N_{0,1}}, \ldots, 1/\sqrt{N_{0,b}}]$. For the joint PMF of the erasure matrix, $P(\mathbf{V})$, we use a simple approximation assuming that entries in $\mathbf{V}$ are independent, i.e.,

$$P(\mathbf{V}) \approx \prod_{b=1}^{B} \prod_{r=1}^{R} P(v_{b,r}). \tag{20}$$

This way, considering $v_{b,r}$ as the virtual binary bit, its bit-wise log-likelihood ratio (LLR) can be defined as

$$\Lambda(v_{b,r}) = \log \frac{P(v_{b,r} = 1)}{P(v_{b,r} = 0)} \tag{21}$$

so that

$$P(v_{b,r}) = \frac{e^{v_{b,r}\Lambda(v_{b,r})}}{1 + e^{\Lambda(v_{b,r})}}. \tag{22}$$

It is convenient, as it simplifies the computations and makes them more stable, to modify the MAP criterion (18) into a log-MAP one:

$$(\hat{\mathbf{x}}, \hat{\mathbf{V}}) \approx \underset{\mathbf{x}\in\chi^B, \mathbf{V}\in\{0,1\}^{R\times B}}{\arg\min} \mathcal{M}(\mathbf{x}, \mathbf{V}), \tag{23}$$

where the objective function $\mathcal{M}(\mathbf{x}, \mathbf{V})$ is defined as

$$\mathcal{M}(\mathbf{x}, \mathbf{V}) \triangleq \left\|\mathbf{y}' - \mathbf{H}'_{\mathrm{eq}}(\mathbf{V}, \mathbf{C})\mathbf{x}\right\|^2 - \sum_{b=1}^{B}\sum_{r=1}^{R} v_{b,r}\Lambda(v_{b,r}) \tag{24}$$

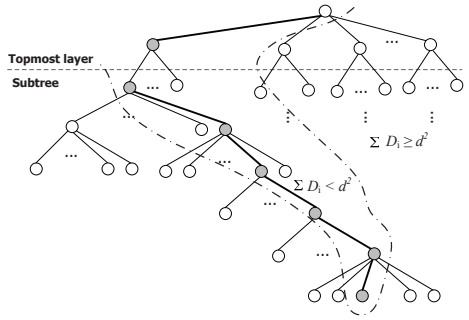

Fig. 4. Tree search structure of the JSD. The topmost layer is dedicated to the detection of $\mathbf{V}$, and the subtree is used for the detection of data packet $\mathbf{x}$.

with the normalization $\mathbf{y}' = \text{diag}(\boldsymbol{\rho})\mathbf{y}$ and $\mathbf{H}'_{\text{eq}}(\mathbf{V},\mathbf{C}) = \text{diag}(\boldsymbol{\rho})\mathbf{H}_{\text{eq}}(\mathbf{V},\mathbf{C})$. Note that the irrelevant constant terms $\log(\pi^{-B}\prod_{b=1}^{B} N_{0,b})$, $\log|\chi|^{-B}$, and $(1+e^{\Lambda(v_{b,r})})^{-1}$, $r = 1,\ldots,R$ and $b = 1,\ldots,B$ are removed. It should be emphasized that, with this objective function, the decoding algorithm duplicates the physical-layer iterative soft-input MIMO decoding algorithm where the *a priori* LLRs of the unknowns are obtained by the channel decoder [36], [37]. Here, the *a priori* probabilities of the erasures are calculated by the approach described in Section IV. However, although the MAP decoding algorithm performs satisfactorily in terms of error rate, its computational complexity may prove prohibitive. For example, choosing $R = B = 4$ and QPSK, the search space has an enormous size 2^{24}. To achieve optimal performance with a lower complexity, we advocate the JSD decoding algorithm described in the next subsection.

B. Joint Sphere Decoding

Sphere decoding is an efficient decoding algorithm that converts an exhaustive search into a constrained tree search [38]–[40]. To apply it to our problem, we structure the tree search of the JSD as shown in Fig. 4, where the topmost layer comprises the $2^{RB}-1$ possible states of $\mathbf{V}$. The subtree for data detection is cascaded below each node of the topmost layer. The objective function (24) is rewritten in the form of an accumulation of partial distances (PDs) D_i:

$$\mathcal{M}(\mathbf{x},\mathbf{V}) = \sum_{i=1}^{B+1} D_i, \tag{25}$$

where the D_i associated with the topmost layer (the $(B+1)$th layer) and the subtree are respectively given by

$$D_{B+1} = -\sum_{b=1}^{B}\sum_{r=1}^{R} v_{b,r}\Lambda(v_{b,r}), \tag{26}$$

$$\sum_{i=1}^{B} D_i = \left\|\mathbf{y}' - \mathbf{H}'_{\text{eq}}(\mathbf{V},\mathbf{C})\mathbf{x}\right\|^2. \tag{27}$$

Eq. (26) shows that the PD of the topmost layer is the summation of the LLRs of $\mathbf{V}$.

After the topmost layer and its PDs are formed, the conventional SD used in physical-layer MIMO receivers can be adopted for data detection. The QR decomposition (QRD) is used to structure a subtree search where x_i and D_i, for $i = 1,\ldots,B$, can be sequentially identified and calculated. Specifically, denoting by $\mathbf{I}_B$ and $(\cdot)^H$ the $B\times B$ identity matrix and the Hermitian transposition, respectively, the QRD transforms the channel matrix into the product of an upper triangular matrix $\mathbf{U}(\mathbf{V},\mathbf{C}) \in \mathbb{C}^{B\times B}$ and a unitary matrix $\mathbf{Q}(\mathbf{V},\mathbf{C}) \in \mathbb{C}^{B\times B}$ as follows:

$$\mathbf{H}'_{\text{eq}}(\mathbf{V},\mathbf{C}) = \mathbf{Q}(\mathbf{V},\mathbf{C})\mathbf{U}(\mathbf{V},\mathbf{C}), \tag{28}$$

where

$$\mathbf{Q}(\mathbf{V},\mathbf{C})^H\mathbf{Q}(\mathbf{V},\mathbf{C}) = \mathbf{I}_B. \tag{29}$$

After multiplying $\mathbf{y}' - \mathbf{H}'_{\text{eq}}(\mathbf{V},\mathbf{C})\mathbf{x}$ by $\mathbf{Q}(\mathbf{V},\mathbf{C})^H$, the objective function (25) becomes

$$\begin{aligned}
&\mathcal{M}(\mathbf{x},\mathbf{V})\\
&= \left\|\mathbf{Q}(\mathbf{V},\mathbf{C})^H\mathbf{y}' - \mathbf{Q}(\mathbf{V},\mathbf{C})^H\mathbf{H}'_{\text{eq}}(\mathbf{V},\mathbf{C})\mathbf{x}\right\|^2 + D_{B+1}\\
&= \left\|\tilde{\mathbf{y}} - \mathbf{U}(\mathbf{V},\mathbf{C})\mathbf{x}\right\|^2 + D_{B+1}\\
&= \sum_{i=1}^{B}\left|\tilde{y}_i - \sum_{j=i+1}^{B} U_{i,j}(\mathbf{V},\mathbf{C})x_j\right|^2 + D_{B+1},
\end{aligned} \tag{30}$$

where $U_{i,j}(\mathbf{V},\mathbf{C})$ and $\tilde{y}_i$ denote the (i,j)th entry of $\mathbf{U}(\mathbf{V},\mathbf{C})$ and the ith entry of $\tilde{\mathbf{y}} = \mathbf{Q}(\mathbf{V},\mathbf{C})^H\mathbf{y}'$, respectively. Using (30), the PD of the subtree for the data detection is given by

$$D_i = \left|\tilde{y}_i - \sum_{j=i+1}^{B} U_{i,j}(\mathbf{V},\mathbf{C})x_j\right|^2, \qquad i = 1,\ldots,B. \tag{31}$$

Then, we confine the search of the JSD by d^2, where d is the radius. Once the accumulated PDs from the topmost layer to the kth layer exceeds the value of d^2, i.e.,

$$\sum_{i=k}^{B+1} D_i \geq d^2, \tag{32}$$

all nodes in the subtree rooted at that node are pruned from the search space. Given that $d^2 \geq \mathcal{M}(\hat{\mathbf{x}},\hat{\mathbf{V}})$, where $(\hat{\mathbf{x}},\hat{\mathbf{V}})$ is the optimal solution defined in (23), the optimal MAP decoding performance can be efficiently achieved.

The search complexity of the subtree can be further reduced by applying the sorted QRD (SQRD) and the Schnorr-Euchner (SE) enumeration [39] which order the nodes along the vertical and horizontal directions, respectively. The SQRD reorders the columns of $\mathbf{U}(\mathbf{V},\mathbf{C})$ to allow the nodes with larger PDs to be visited at upper layers, resulting in earlier tree pruning. The SE enumeration orders the nodes rooted from the same parent node with ascending PDs. By using the SQRD and the SE enumeration, once a visited node in the topmost layer has a PD larger than the squared radius d^2, all the unvisited nodes in the topmost layer are guaranteed to have PDs larger than d^2. Therefore, the JSD can be terminated without losing optimality. In other words, though the JSD comprises $RB-1$ conventional SDs for the subtrees in the worst case, the average complexity is considerably lowered since many subtrees are not visited.

Last, it should be emphasized that, with the JSD, the receiver can gather probabilistic information about $\mathbf{V}$. By using

this on-line learning process, the destination node can sense and track the variation of δ, which is particularly important when the channel statistics are dynamic.

C. MMSE–Sorted QR Decomposition

The average decoding complexity with SD is known to increase when the channel matrix is ill-conditioned [41]. Now, due to erasures, this situation occurs more often in the end-to-end transmission of ad hoc CRNs than on physical-layer MIMO channels. To mitigate this effect, we apply MMSE-SQRD to regularize the channel matrix. Specifically, MMSE-SQRD performs the following operation [42]:

$$\begin{bmatrix} \mathbf{H}'_{\text{eq}}(\mathbf{V},\mathbf{C}) \\ \sigma_x^2 \text{diag}(\mathbf{1}) \end{bmatrix} \mathbf{P}_{\text{MMSE}}(\mathbf{V},\mathbf{C}) = \underbrace{\begin{bmatrix} \mathbf{Q}_{\text{MMSE},1}(\mathbf{V},\mathbf{C}) \\ \mathbf{Q}_{\text{MMSE},2}(\mathbf{V},\mathbf{C}) \end{bmatrix}}_{\mathbf{Q}_{\text{MMSE}}(\mathbf{V},\mathbf{C})} \mathbf{U}_{\text{MMSE}}(\mathbf{V},\mathbf{C}), \tag{33}$$

where $\mathbf{U}_{\text{MMSE}}(\mathbf{V},\mathbf{C}) \in \mathbb{C}^{B\times B}$ denotes the upper triangular matrix, and $\mathbf{P}_{\text{MMSE}}(\mathbf{V},\mathbf{C}) \in \{0,1\}^{B\times B}$ is the permutation matrix for sorting. The orthonormal matrix $\mathbf{Q}_{\text{MMSE}}(\mathbf{V},\mathbf{C}) \in \mathbb{C}^{2B\times B}$ is partitioned into two square matrices $\mathbf{Q}_{\text{MMSE},1}(\mathbf{V},\mathbf{C})$, $\mathbf{Q}_{\text{MMSE},2}(\mathbf{V},\mathbf{C}) \in \mathbb{C}^{B\times B}$. Multiplying $\mathbf{Q}_{\text{MMSE},1}(\mathbf{V},\mathbf{C})^H$ by $\mathbf{y}'$, we write

$$\begin{aligned} &\mathbf{Q}_{\text{MMSE},1}(\mathbf{V},\mathbf{C})^{\text{H}}\mathbf{y}' = \\ &\mathbf{U}_{\text{MMSE}}(\mathbf{V},\mathbf{C})\mathbf{P}_{\text{MMSE}}(\mathbf{V},\mathbf{C})^H\mathbf{x} \\ &+\left(-\frac{1}{\sigma_x}\mathbf{Q}_{\text{MMSE},2}(\mathbf{V},\mathbf{C})^{\text{H}}\mathbf{x}+\mathbf{Q}_{\text{MMSE},1}(\mathbf{V},\mathbf{C})^{\text{H}}\mathbf{n}\right), \end{aligned} \tag{34}$$

where the terms in the bracket in the right-hand side include the interference term degrading the algorithm performance. Nevertheless, this interference can be cancelled during the tree search [43]. By applying MMSE-SQRD, we generate new PDs for the subtree, which reduces the decoding complexity.

VI. Simulation Results

In this section, the performance of the proposed system is evaluated, and its analysis validated, by means of Monte Carlo simulations. The fading gains $g_{b,r}$ are assumed to be the product of N_r i.i.d. complex Gaussian random variables. The noise power spectral density $N_{0,b}$ is assumed to be the same for all time instants. In order to verify the analysis of the erasure probability and to demonstrate the capability of the proposed pipeline scheduling, only the erasures resulting from the packet expiration are considered.

Assume equal waiting periods $W = 3$, $B = 3$, and $N_r = 3$. Fig. 5 shows the erasure probability of the pipeline scheduling scheme. The close agreement between numerical and analytical results of $P(v_{b,r})$ validates our analyses. As $P(v_{1,r})$ takes the same value for conventional and pipeline scheduling, the improvement offered by pipeline scheduling can be observed from the gap between $P(v_{1,r})$ and $P(v_{3,r})$. For $\delta = 0.3$, the probability of path availability increases from 0.35 to 0.88, proving the effectiveness of the pipeline scheduling scheme. Additionally, the comparison between numerical and analytical values of $P(\mathbf{v}_r = [1\ 1\ 1])$ shows the accuracy of the approximation (20).

Fig. 6 considers the situation with $N_r = 2$, $R = B = 4$, equal waiting period $W = 4$, and QPSK modulation. The receiver has perfect knowledge of $\mathbf{V}$. The numerical results compare various PTCs by showing their bit error rate (BER). The performances of coded transmission with orthonormal coding matrix and of uncoded transmission are used as baselines. While the orthonormal coding matrix [20] reduces the error floor as compared with uncoded transmission, DFT-based PTC delivers a more remarkable performance improvement.

Fig. 7 refers to almost the same situation as Fig. 6, except that the PTC is fixed to DFT-based and the scheduling schemes are changed. At BER$= 10^{-3}$, pipeline scheduling with $\delta = 0.7$ enhances the SNR by more than 10 dB as compared to conventional scheduling, while the scheme using unequal waiting periods brings in an additional 2 dB improvement. According to [20], the unequal waiting periods [6 4 3 3] are adjusted to minimize the geometric mean of $P(v_{b,r} = 0)$, $r = 1,\ldots,R$. It should be emphasized that, from these simulations, both DFT-based PTC and pipeline scheduling with unequal waiting periods perform better for larger δ.

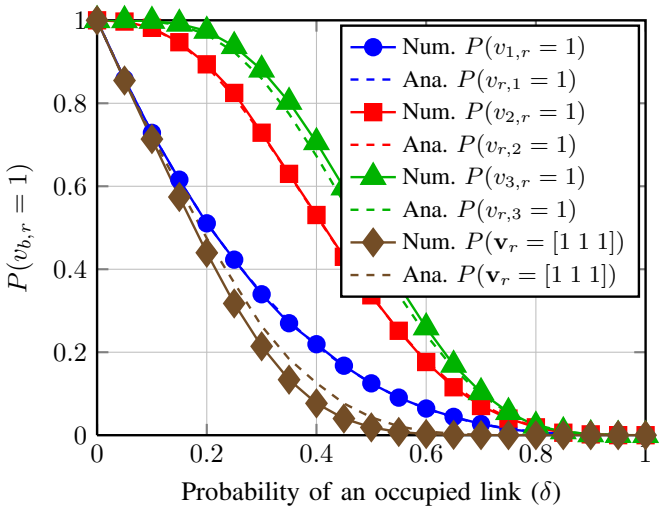

Fig. 5. Validation of erasure-probability analysis. The parameters used are $N_r = 3$, $B = 3$, and equal waiting period $W = 3$.

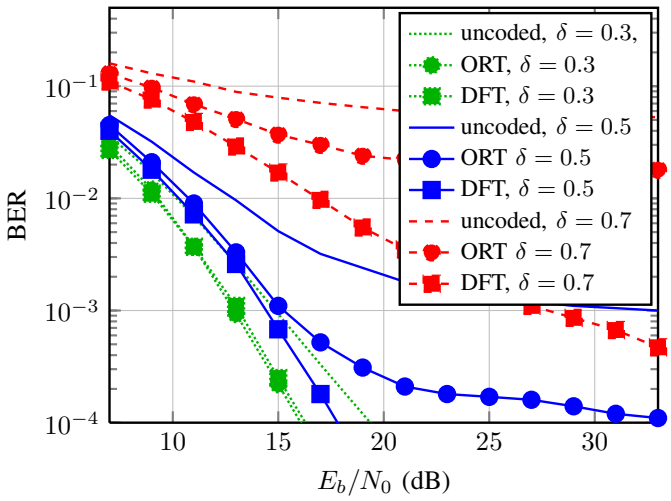

Fig. 6. BER performance of end-to-end uncoded and coded transmission. Orthonormal coding matrix (ORT) and DFT-based PTC are compared. The parameters used are $N_r = 2$, and $R = B = 4$; QPSK and the pipeline scheduling scheme with equal waiting period $W = 4$ are adopted.

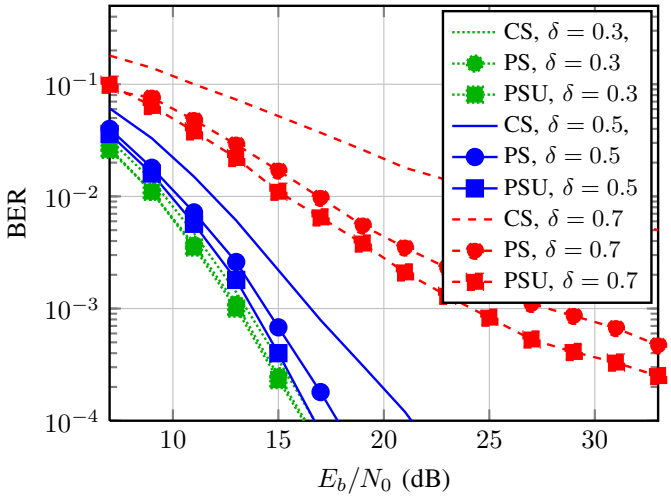

Fig. 7. BER performance for conventional scheduling (CS), pipeline scheduling (PS), and pipeline scheduling with unequal waiting periods (PSU) [6 4 3 3]. The parameters used are $N_r = 2$, and $R = B = 4$; QPSK and DFT-based PTC are adopted.

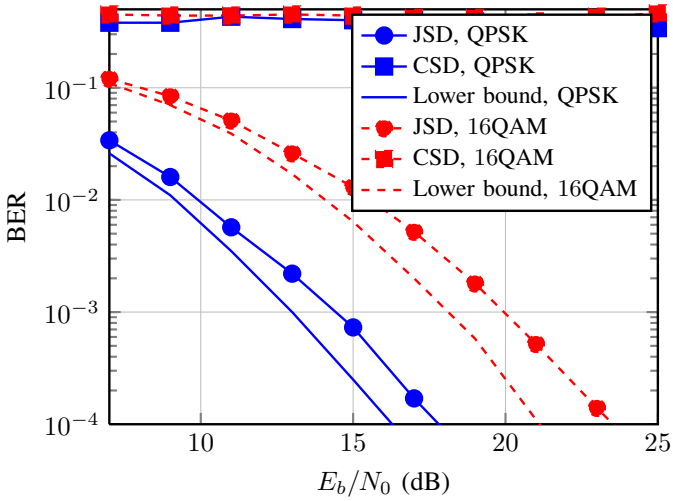

Fig. 8. BER of JSD, conventional SD (CSD), and the lower bound. The parameters used are $N_r = 2$, $R = B = 4$, and $\delta = 0.3$; DFT-based PTC and the pipeline scheduling scheme with unequal waiting periods [6 4 3 3] are adopted.

This implies that these techniques are more effective in a high-spectral-efficiency scenario, which is aligned with future trends in wireless communications. In particular, pipeline scheduling can increase spectrum efficiency just thanks to its aggressive sensing and access strategy.

The additional simulation charts show BER and complexity of the decoding algorithm. The transmission uses a DFT-based PTC and pipeline scheduling with unequal waiting periods [6 4 3 3]. The parameters chosen are $N_r = 2$, $R = B = 4$, and $\delta = 0.3$. The JSD assumes knowledge of (δ, N_r), and is allowed to estimate the *a priori* probability of $\mathbf{V}$ by using the approach outlined in Section IV. For data detection, SD adopts the depth-first tree search algorithm with a radius update matched to hard-output MIMO detection [44]. The lower bound is obtained from the decoder having perfect knowledge of $\mathbf{V}$, i.e., when only the subtree with right $\mathbf{V}$ is traversed. The conventional SD (CSD) without knowledge of

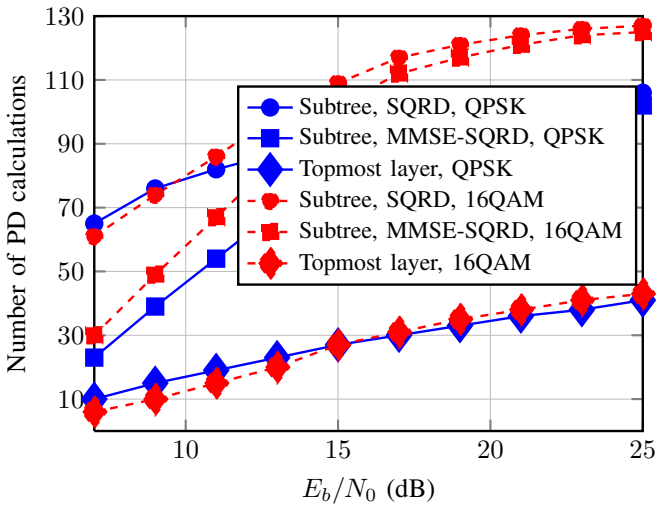

Fig. 9. Decoding complexity of JSD with SQRD and MMSE-SQRD channel preprocessing. The parameters used are $N_r = 2$, $R = B = 4$, and $\delta = 0.3$; DFT-based PTC and the pipeline scheduling scheme with unequal waiting periods [6 4 3 3] are adopted.

the *a priori* probability of $\mathbf{V}$ is used as baseline. In detail, the CSD follows the maximum likelihood (ML) criterion, which is optimal for physical-layer noniterative MIMO decoding. As shown in Fig. 8, while the JSD approaches the lower bound for both QPSK and 16QAM, the CSD fails to correctly detect the data packets, since it assumes $\Lambda(v_{b,r}) = 0$. Fig. 9 depicts the number of PD calculations, intended as a complexity measure. It is interesting to observe that the complexity increases when SNR increases, which is counter-intuitive. Such phenomenon is explained by observing the trend of the number of PD calculations of the topmost layer. Since N_0 decreases as SNR increases, D_{B+1} in (26) becomes relatively smaller at high SNR, so that more nodes in the topmost layer satisfy the radius constraint. The trees are only pruned when the subtrees are traversed. Nonetheless, the largest number of PD calculations at the topmost layer is still much smaller than $2^{RB} - 1$ ($40 \ll 2^{16} - 1$), as with an SE enumeration. The minimum number of PD calculations for traversing the subtree to the bottommost layer is $2B - 1$, where B and $B - 1$ PD calculations are used for the forward and backward searches, respectively [28]. For the configurations in Fig. 9, the average numbers of the PD calculations per subtree are mostly smaller than $2B - 1$, indicating that many subtree searches are terminated before reaching the bottommost layer. Comparing the results of using SQRD and MMSE-SQRD as depicted in Fig. 9, MMSE-SQRD is more efficient at low SNR. This is because MMSE-SQRD can mitigate the noise enhancement caused by an ill-conditioned channel matrix, which is especially severe at low SNR.

VII. Conclusion

In this paper, we advocate a novel virtual MIMO system as a model for ad hoc CRNs. The uncertainty intrinsic in the opportunistic use of links is modeled by random erasures. Based on this virtual MIMO formulation, several transmission techniques are proposed to deal with fast-erasure channels. A pipeline scheduling scheme is introduced to reduce the erasure

probability. PTC and JSD play central roles at source and destination nodes, respectively, for encoding and decoding. The latter is derived from the MAP criterion, but needs a much lower average complexity, especially in combination with the MMSE-SQRD. Thanks to the proposed techniques, reliable CR communication from source to destination is made possible through multipath multihop wireless networking. Neither the dedicated spectrum nor the feedback control with bi-directional link signaling is needed for general applications. We should also emphasize that, although this work specifically deals with ad hoc CRNs, its scope is actually wider, as this virtual MIMO concept is actually applicable to a general class of ad hoc networks. We believe that the research reported here will open new avenues for future research on innovative coding schemes and decoding algorithms for virtual MIMO systems at/above network layer.

ACKNOWLEDGMENTS

The authors would like to thank the editor and the anonymous reviewers for their constructive suggestions that lead to the significant enhancement of the presentation of this paper.

REFERENCES

[1] J. Mitola III, "Cognitive radio for flexible mobile multimedia communications," in *Proc. 1999 IEEE Int. Workshop Mobile Multimedia Commun.*

[2] J. Mitola III and J. G. Q. Maguire, "Cognitive radio: making software radios more personal," *IEEE Personal Commun.*, vol. 6, no. 4, pp. 13–18, Aug. 1999.

[3] S. Haykin, "Cognitive radio: brain-empowered wireless communications," *IEEE J. Sel. Areas Commun.*, vol. 23, no. 2, pp. 201–220, Feb. 2005.

[4] K.-C. Chen and R. Prasad, *Cognitive Radio Networks*. John Wiley & Sons, 2009.

[5] E. Biglieri, A. J. Goldsmith, L. J. Greenstein, N. B. Mandayam, and H. V. Poor, *Principles of Cognitive Radio*. Cambridge University Press, 2013.

[6] K.-C. Chen, B. K. Cetin, Y.-C. Peng, N. Prasad, J. Wang, and S. Lee, "Routing for cognitive radio networks consisting of opportunistic links," in *Wirel. Commun. Mob. Comput. (John Wiley)*, Aug. 2009, pp. 451–466.

[7] K. Yang and X. Wang, "Cross-layer network planning for multi-radio multi-channel cognitive wireless networks," *IEEE Trans. Commun.*, vol. 56, no. 10, pp. 1705–1714, Oct. 2008.

[8] L. Ding, T. Melodia, S. N. Batalama, J. D. Matyjas, and M. J. Medley, "Cross-layer routing and dynamic spectrum allocation in cognitive radio ad hoc networks," *IEEE Trans. Veh. Technol.*, vol. 59, no. 4, pp. 1969–1979, May 2010.

[9] M. Caleffi, I. F. Akyildiz, and L. Paura, "OPERA: optimal routing metric for cognitive radio ad hoc networks," *IEEE Trans. Wireless Commun.*, vol. 11, no. 8, pp. 2884–2894, Apr. 2012.

[10] B. Mumey, J. Tang, I. R. Judson, and D. Stevens, "On routing and channel selection in cognitive radio mesh networks," *IEEE Trans. Veh. Technol.*, vol. 61, no. 9, pp. 4118–4128, Nov. 2012.

[11] A. Azarfar, J.-F. Frigon, and B. Sansò, "Improving the reliability of wireless networks using cognitive radios," *IEEE Commun. Surveys Tuts.*, vol. 14, no. 2, pp. 338–354, May 2012.

[12] K.-C. Chen and S.-Y. Lien, "Machine-to-machine communications: technologies and challenges ," *Ad Hoc Netw.*, Mar. 2013.

[13] S.-C. Lin and K. Chen, "Spectrum aware opportunistic routing in cognitive radio networks," in *Proc. 2010 IEEE Glob. Commun. Conf.*

[14] K. R. Chowdhury and I. F. Akyildiz, "CRP: a routing protocol for cognitive radio ad hoc networks," *IEEE J. Sel. Areas Commun.*, vol. 29, no. 4, pp. 794–804, Apr. 2011.

[15] Y. Liu, L. X. Cai, and X. Shen, "Spectrum-aware opportunistic routing in multi-hop cognitive radio networks," *IEEE J. Sel. Areas Commun.*, vol. 30, no. 10, pp. 1958–1968, Nov. 2012.

[16] P.-Y. Chen, W.-C. Ao, and K.-C. Chen, "Rate-delay enhanced multipath transmission scheme via network coding in multihop networks," *IEEE Commun. Lett.*, vol. 16, no. 3, pp. 281–283, Mar. 2012.

[17] M. K. Marina and S. R. Das, "On-demand multipath distance vector routing in ad hoc networks," in *Proc. 2001 IEEE Int. Conf. Netw. Protocol.*

[18] P. Djukic and S. Valaee, "Reliable packet transmissions in multipath routed wireless networks," vol. 5, no. 5, pp. 548–559, May 2006.

[19] S. Fashandi, S. O. Gharan, and A. K. Khandani, "Path diversity over packet switched networks: performance analysis and rate allocation," vol. 18, no. 5, pp. 1373–1386, May 2010.

[20] I.-W. Lai, C.-H. Lee, and K.-C. Chen, "A virtual MIMO path-time code for cognitive ad hoc networks," *IEEE Commun. Lett.*, vol. 17, no. 1, pp. 4–7, Jan. 2013.

[21] S. K. Jayaweera, "Virtual MIMO based cooperative communication for energy-constrained wireless sensor networks," *IEEE Trans. Wireless Commun.*, vol. 5, no. 5, pp. 984–989, May 2006.

[22] D. Gesbert, S. Hanly, H. Huang, S. Shamai (Shitz), O. Simeone, and W. Yu, "Multi-cell MIMO cooperative networks: a new look at interference," *IEEE J. Sel. Areas Commun.*, vol. 28, no. 9, pp. 1380–1408, May 2010.

[23] J. N. Laneman and G. W. Wornell, "Distributed space-time-coded protocols for exploiting cooperative diversity in wireless networks," *IEEE Trans. Inf. Theory*, vol. 49, no. 10, pp. 2415–2425, Oct. 2003.

[24] R. U. Nabar, H. Bölcskei, and F. W. Kneubühler, "Fading relay channels: performance limits and space-time signal design," *IEEE J. Sel. Areas Commun.*, vol. 22, no. 6, pp. 1099–1109, Aug. 2004.

[25] Y. Jing and B. Hassibi, "Distributed space-time coding in wireless relay networks," *IEEE Trans. Wireless Commun.*, vol. 5, no. 12, pp. 3524–3536, Dec. 2006.

[26] F. Oggier and B. Hassibi, "An algebraic coding scheme for wireless relay networks with multiple antenna nodes," *IEEE Trans. Signal Process.*, vol. 56, no. 7, pp. 2957–2966, July 2008.

[27] B. Rankov and A. Wittneben, "Distributed spatial multiplexing in wireless networks," in *Proc. 2004 Asilomar Conf. Signals, Syst., Comput.*

[28] T.-D. Chiueh, P.-Y. Tsai, and I.-W. Lai, *Baseband Receiver Design for Wireless MIMO-OFDM Communications*. Wiley-IEEE Press, 2012.

[29] M. G. Khoshkholgh, K. Navaie, and H. Yanikomeroglu, "On the impact of the primary network activity on the achievable capacity of spectrum sharing over fading channels," *IEEE Trans. Wireless Commun.*, vol. 8, no. 4, pp. 2100–2111, Apr. 2009.

[30] D. Gross and C. M. Harris, *Fundamentals of Queueing Theory*, 4th ed. Wiley-Interscience, 2008.

[31] W.-C. Ao and K.-C. Chen, "End-to-end HARQ in cognitive radio network," in *Proc. 2010 IEEE Wireless Commun. Netw. Conf.*

[32] E. Biglieri, *Coding for Wireless Channels*. Springer, 2005.

[33] V. Tarokh, N. Seshadri, and A. R. Calderbank, "Space-time codes for high data rate wireless communication: performance criterion and code construction," *IEEE Trans. Inf. Theory*, vol. 44, no. 2, pp. 744–765, Mar. 1998.

[34] Y.-Y. Lin and K.-C. Chen, "Asynchronous dynamic spectrum access," *IEEE Trans. Veh. Technol.*, vol. 61, no. 1, pp. 222–236, Jan. 2012.

[35] First Report and Order, Federal Communication Commission Std, FCC 02-48, Feb. 2002.

[36] B. M. Hochwald and S. ten Brink, "Achieving near-capacity on a multiple-antenna channel," *IEEE Trans. Commun.*, vol. 51, no. 3, pp. 389–399, Mar. 2003.

[37] H. Vikalo, B. Hassibi, and T. Kailath, "Iterative decoding for MIMO channels via modified sphere decoder," *IEEE Trans. Wireless Commun.*, vol. 3, no. 6, pp. 2299–2311, May 2004.

[38] E. Viterbo and E. Biglieri, "A universal decoding algorithm for lattice codes," in *Proc. 1993 GRETSI Symp.*.

[39] C. P. Schnorr and M. Euchner, "Lattice basis reduction: improved practical algorithms and solving subset sum problems," *Math. Programming*, vol. 66, pp. 181–191, Aug. 1994.

[40] L. G. Barbero and J. S. Thompson, "Fixing the complexity of the sphere decoder for MIMO detection," *IEEE Trans. Wireless Commun.*, vol. 7, no. 6, pp. 2131–2142, June 2008.

[41] C. Studer, A. Burg, and H. Bölcskei, "Soft-output sphere decoding: algorithms and VLSI implementation," *IEEE J. Sel. Areas Commun.*, vol. 26, no. 2, pp. 290–300, Feb. 2008.

[42] D. Wübben, R. Böhnke, V. Kühn, and K. Kammeyer, "MMSE extension of V-BLAST based on sorted QR decomposition," in *Proc. 2003 IEEE Veh. Technol. Conf. – Fall*.

[43] C. Studer and H. Bölcskei, "Soft-input soft-output single tree-search sphere decoding," *IEEE Trans. Inf. Theory*, vol. 56, no. 10, pp. 4827–4842, Oct. 2010.

[44] E. Agrell, T. Eriksson, A. Vardy, and K. Zeger, "Closest point search in lattices," *IEEE Trans. Inf. Theory*, vol. 48, no. 8, pp. 2201–2214, Aug. 2002.

I-Wei Lai (M'11) received his Ph.D. in electrical engineering from the Graduate Institute of Electronics Engineering (GIEE) at National Taiwan University (NTU) in 2011, and he is now a Postdoctoral Researcher at Research Center for Information Technology Innovation (CITI), Academia Sinica, Taipei, Taiwan. He was a Research Assistant with the Institute of Integrated Signal Processing Systems, RWTH Aachen University, Aachen, Germany. He was the recipient of the GIEE-NTU best thesis award in 2011 for his Ph.D. thesis and is a member of Phi Tau Phi Scholastic Honor Society. His research interests include baseband signal processing, optimization, MIMO communication, and ad hoc cognitive radio network.

Chien-Lun Chen received the B.S. degree from the National Tsing-Hua University, Hsinchu, Taiwan, in 2004, and the M.S. degree in electrical engineering from the National Taiwan University, Taipei, Taiwan, in 2009. He was a research associate with the Telecommunications Research Center, National Taiwan University from August 2009 to June 2010. He is currently a Ph.D. student in Ming Hsieh Department of Electrical Engineering in University of Southern California, Los Angeles, California, from August 2010. His research interests include wireless communications, cooperative communications, stochastic control and information theory.

Chia-Han Lee received his B.S. degree from National Taiwan University, Taipei, Taiwan in 1999, M.S. degree from the University of Michigan, Ann Arbor in 2003, and Ph.D. from Princeton University in 2008, all in electrical engineering. From 1999 to 2001, he served in the R.O.C. army as a missile operations officer. From 2008 to 2009, he was a postdoctoral research associate at the University of Notre Dame, USA. Since 2010, he has been with Academia Sinica, Taipei, Taiwan, as an Assistant Research Fellow. His research interests include wireless communications, wireless networks, and signal processing.

Kwang-Cheng Chen (M'89-SM'94-F'07) received B.S. from the National Taiwan University in 1983, M.S. and Ph.D from the University of Maryland, College Park, United States, in 1987 and 1989, all in electrical engineering. From 1987 to 1998, Dr. Chen worked with SSE, COMSAT, IBM Thomas J. Watson Research Center, and National Tsing Hua University, in mobile communications and networks. Since 1998, Dr. Chen has been with National Taiwan University, Taipei, Taiwan, ROC, and is the Distinguished Professor and Deputy Dean in academic affairs for the College of Electrical Engineering and Computer Science, National Taiwan University. Dr. Chen actively involves organization of various IEEE conferences as General/TPC chair/co-chair. He has served editorship with a few IEEE journals and many international journals and served various positions in IEEE. Dr. Chen also actively participates and has contributed essential technology to various IEEE 802, Bluetooth, and 3GPP wireless standards. He has authored and co-authored over 250 technical papers and more than 20 granted US patents. He co-edits (with R. DeMarca) the book *Mobile WiMAX* published by Wiley 2008, and authors a book *Principles of Communications* published by River 2009, and co-author (with R. Prasad) another book *Cognitive Radio Networks* published by Wiley 2009. Dr. Chen is an IEEE Fellow and has received a number of awards including 2011 IEEE COMSOC WTC Recognition Award and co-authored a few award-winning papers published in the IEEE ComSoc journals and conferences. Dr. Chen's research interests include wireless communications and network science.

Ezio Biglieri (M'73 - SM'82 - F'89 - LF'10) was born in Aosta (Italy). He received his training in Electrical Engineering from Politecnico di Torino (Italy), where he received his Dr. Engr. degree in 1967. He was elected three times to the Board of Governors of the IEEE Information Theory Society, and in 1999 he was the President of the Society. He is serving on the Scientific Board of the French company Sequans Communications, and, till 2012, he was a member of the Scientific Council of the "Groupe des Ecoles des Telecommunications" (GET), France. Since 2011 he has been a member of the Scientific Advisory Board of CHIST-ERA (European Coordinated Research on Long-term Challenges in Information and Communication Sciences & Technologies ERA-Net). In the past, he was Editor-in-Chief of the IEEE TRANSACTIONS ON INFORMATION THEORY, IEEE COMMU- NICATIONS LETTERS, the *European Transactions on Telecommunications*, and the *Journal of Communications and Networks*. He is a Life Fellow of the IEEE. Among other honors, he received the IEEE Donald G. Fink Prize Paper Award (2000), the IEEE Third-Millennium Medal (2000), the IEEE Communications Society Edwin Howard Armstrong Achievement Award (2001), the Journal of Communications and Networks Best Paper Award (2004 and 2012), the IEEE Information Theory Society Aaron D. Wyner Distinguished Service Award (2012), and the EURASIP Athanasios Papoulis Award for outstanding contributions to education in communications and information theory (2013).